ACS Photonics

Article

pubs.acs.org/journal/apchd5

Quantum Efficiency of Organic Solar Cells: Electro-Optical Cavity Considerations

Ardalan Armin, Marappan Velusamy, Pascal Wolfer, Yuliang Zhang, Paul L Burn, Paul Meredith,* and Almantas Pivrikas

Centre for Organic Photonics & Electronics (COPE), School of Mathematics and Physics and School of Chemistry and Molecular Biosciences, The University of Queensland, Brisbane 4072, Australia

Supporting Information

ABSTRACT: Organic solar cells (OSCs) are composed of one or more layers of order 100 nm thickness sandwiched between metallic and transparent electrodes. As such, they are low finesse, multilayer optical cavities where the optical field distribution is governed by the complex refractive indices and thicknesses of all layers in the "solar cell stack". Optical interference and parasitic absorbance in nonactive layers can have a dramatic effect on the shape of the measured external quantum efficiency (EQE), the parameter often used to optimize device structure and derive critical insight regarding charge generation and extraction. In this communication, we study a model high efficiency OSC system (PCDTBT/PC70BM) as a function of active layer thickness, blend composition and processing. The spectral shapes of the measured EQEs show strong thickness and blend ratio dependence. However, when correctly determined, the internal quantum efficiencies (IQEs) are spectrally flat. The differences in EQE spectral shape predominantly originate from optical interference and parasitic absorptions rather than charge generation or transport phenomena. We also demonstrate similar results for a second model system (PCPDTBT/PC60BM) in which an energy-dependent "IQE-like" response has recently been used to justify the existence of hot excitons. Once again, we show the origin of these spectral phenomena to be optical, not electronic. These cases highlight the fact that thin film organic solar cells (even single junction) must be properly considered as low finesse electro-optical cavities, a point that is not universally appreciated.

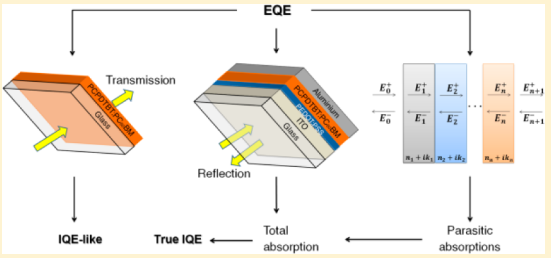

KEYWORDS: *organic solar cell, low finesse electro-optical cavities, internal quantum efficiency, hot exciton, parasitic absorption, optical interference*

INTRODUCTION

Over the past few years, the power conversion efficiencies (PCEs) of organic solar cells (OSCs) have been steadily improving[1,2] with the current state-of-the-art exceeding 9%.[3] These improvements in both single and multiple junction architectures stem from a number of innovations, namely, (i) the development of novel[4] narrow optical gap (macro)molecules that allow harvesting of photons over a broad spectral range into the near-infrared;[3,5,6] (ii) enhanced light absorption in the active layer (the bulk heterojunction layer);[7,8] (iii) better charge collection afforded by junction structuring;[9] and (iv) materials and composition optimization[10] to increase the internal quantum efficiency.[11]

The performance of any solar cell or photodiode is largely governed by the incident photon to converted electron efficiency (η_{IPCE}), that is, the externally measured ratio of the number of collected charges to the number of incident photons often referred to as the external quantum efficiency (EQE). To achieve the theoretical upper limit of the PCE (the so-called thermodynamic or Shockley-Quiesser limit[12] requires simultaneous optimization of the internal quantum efficiency (IQE) and optical absorption over the solar spectral window. As described by Forrest et al.[13] this interdependency can be expressed as

$$\eta_{IPCE} = \eta_A \eta_{IQE} \quad (1)$$

where η_{IQE} is the fractional internal quantum efficiency, that is, the ratio of the number of collected charges to the number of photons absorbed by the junction and η_A represents the amount of incident light that is absorbed by the active region. Considering that organic semiconductors typically exhibit charge carrier mobilities orders of magnitude less than their inorganic counterparts,[14] it is conventionally thought that a high η_{IQE} can only be realized with thin junctions that allow efficient charge collection.[1,15,16] The upper thickness limit of the active layer for efficient charge collection is defined by the carrier transit time and lifetime.[17] For most solution processed organic solar cells based on the common bulk-heterojunction (BHJ) architecture, the optimum thickness is of order ~100 nm, that is, on a similar dimension to the wavelength of visible light.[15,16,18] Consequently, the optical field distribution in the active layer is not simply Beer–Lambert (exponentially decaying across the film) because cavity interference becomes important due to reflecting back electrodes.[19,20] In such a case, the optical field distribution

Received: September 18, 2013
Published: February 13, 2014

(which defines the photogenerated carrier profile)[21] is strongly wavelength-dependent and is governed by the optical characteristics of the solar cell stack, that is, the complex index of refraction ($n + ik$) and the thickness of all layers. Hence, variations in these properties affect the solar cell performance, in particular, the shape of the external quantum efficiency (EQE).

When faced with a new material or combination of materials, a common approach to optimizing the device architecture is to perform a single variable analysis of the donor−acceptor blend ratio,[22] junction thickness, and processing parameters (such as solvents,[23] polymer molecular weight,[24,25] annealing, additives,[26] and doping[27]). Standard white light PCE and EQE measurements can then be used to assess the device performance as a function of all variables and to empirically arrive at an "optimized" outcome. However, first-order parameters such as junction thickness and blend composition directly impact the optical field distribution via the optical constants and, hence, the efficiency of carrier photogeneration and the shape of the spectral response. Knowledge of n, k, and d for all layers in the stack allows one to perform simulations of the likely field distribution in the junction and helps in disentangling the electrical and optical effects.[28] However, it is important to note that the simulations only provide insight into optical effects, and details of the charge transport and exciton dissociation efficiencies are needed to gain a complete picture of charge generation and extraction.[29] Furthermore, the shape of the EQE (and more importantly the IQE) has recently been used to understand the likely mechanisms for free carrier generation. For example, Grancini et al.[30] reported that an apparent energy dependence in the IQE spectrum proved the existence of a hot exciton effect in PCPDTBT-based organic solar cells. However, both Armin et al.[31] and Scharber[32] have shown the IQE is in fact spectrally flat when cavity interference and parasitic absorptions are properly accounted for. Hence, from a device optimization and mechanistic perspective these apparently "passive" optical effects must be understood and accounted for.

In this current study we clearly demonstrate the impact of cavity interference and parasitic absorption effects in two model organic solar cell systems: (i) PCDTBT/PC70BM (poly[*N*-9″-heptadecanyl-2,7-carbazole-*alt*-5,5-(4′,7′-di-2-thienyl-2′,1′,3′-benzothiadiazole)]/phenyl-C71-butyric acid methyl ester); and (ii) PCPDTBT/PC60BM (poly[2,6-(4,4-bis-{2-ethylhexyl}-4*H*-cyclopenta[2,1-*b*;3,4-*b*′]-dithiophene)-*alt*-4,7-(2,1,3-benzothiadiazole)]/phenyl-C61-butyric acid methyl ester). In the former case we exemplify a device optimization analysis (blend ratio and active layer thickness) and show the dominant role the junction thickness plays on the shape of the EQE. We also demonstrate that the quantum efficiency is not limited by charge transport and recombination up to an active layer thickness of 120 nm, and that the IQE response is incident energy independent (i.e., spectrally flat) when correctly determined via EQE, reflectance, and ellipsometric n, k, and d measurements in combination with transfer matrix simulations. We confirm similar findings in the PCPDTBT system and, in particular, confirm the spectrally flat nature of the IQE.

RESULTS AND DISCUSSION

PCDTBT/PC70BM Blend Ratio. To demonstrate the effect of donor−acceptor blend ratio on device performance and spectral characteristics, a typical example of OPV performance optimization, PCDTBT/PC70BM bulk heterojunction (BHJ) solar cells of different compositions were fabricated in an inert environment (<1 ppm H_2O and O_2) by spin-casting solutions of constant total active component concentration (see the Experimental Section for full details). Standard white-light AM1.5G current−voltage curves and monochromatic External Quantum Efficiencies (EQE) were measured under carefully controlled conditions (see Supporting Information, Figures S1 and S2 and Experimental Section), and power conversion efficiencies of between 1.5 and 6.0% were achieved, consistent with previous reports.[15] The blend ratio of 1:4 by weight (PCDTBT/PC70BM) was affirmed to be the most efficient, in agreement with the bulk of published literature.[15,16,31] As demonstrated in Figure 1a, the shape of the EQE spectrum

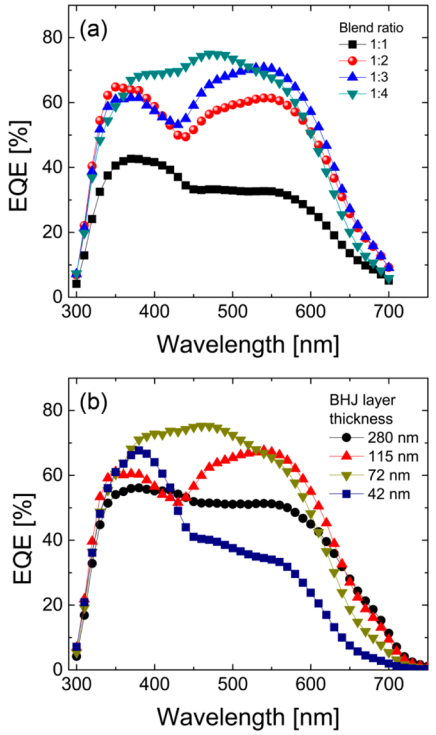

Figure 1. EQE spectra of PCDTBT/PC70BM organic solar cells: (a) Measurements in devices with various blend ratios of acceptor to donor; (b) Measurements in devices with a fixed blend ratio of 1:4 and different thicknesses of the active layer. The similarity between EQE spectra in figures (a) and (b) suggests that the action spectra are mainly governed by the active layer thickness and not by the blend ratio.

changes as a function of blend ratio. The fact that each junction is of a different thickness (note the active layers were cast under identical spin-casting conditions) makes the optimization process very difficult in this single variable experiment. It is worth noting that the 1:4 blend has the flattest and highest peak EQE and this is often taken as the point at which the highest possible efficiency in a "balanced device" is achieved.[31]

PCDTBT/PC70BM Junction Thickness. The thickness of the solar cell active layer has a first order effect on the spectral dependence of the EQE below the Beer−Lambert limit. To demonstrate this phenomenon, PCDTBT/PC70BM devices were fabricated at a fixed blend ratio of 1:4 with different junction thickness produced by varying the deposition spin-casting speed and solution concentrations (see Experimental Section). In Figure 1b we show EQEs over a range of thicknesses, including a "thick junction" (280 nm) for which the absorption spectrum is flat (due to the optical density being high across the response spectrum), leading to a relatively flat EQE. Once again, the different junction thicknesses deliver very different EQE spectral

dx.doi.org/10.1021/ph400044k | ACS Photonics 2014, 1, 173−181

dependencies. This clearly demonstrates the difficulty associated with optimizing the device based upon these two single variable experiments and the interdependency in both cases of the EQE on $\eta_A(\lambda)$. An important question to answer is whether the blend ratio effects are merely a consequence of the different junction thicknesses caused in the PCDTBT/PC70BM system by variations in spin-casting solution viscosity as a function of polymer concentration. We will return to this question later.

Optical Constants Determination and Cavity Modeling. Detailed knowledge of the optical constants (n and k) of all layers in the solar cell stack (including the active layer as a function of blend ratio) allows one to determine via transfer matrix calculations the distribution of the optical field in the "cavity" that is the junction. In particular, such simulations can be used to predict the active layer thickness at which the optical field distribution at the predicted peak EQE is positioned in the center of the junction region to minimize losses associated with exciton quenching by free charge carriers. Furthermore, tuning of the cavity effects (with for example the use of an optical spacer[34,35]) could be used to amplify the most efficient photocurrent generating pathway in a device where both Channel I and Channel II processes are operating as a function of incident light energy.[36] We have employed spectroscopic ellipsometry to determine accurate optical constants (n and k) for the PCDTBT/PC70BM films as a function of blend ratio (see Experimental Section). It is important to note that our ellipsometric n and k analysis used films with different thicknesses to avoid any issues with a morphology-induced thickness dependence of the optical constants. We did not observe this in the PCDTBT/PC70BM system. The results of these measurements are shown in Figure 2a [k] and b [n]. Films

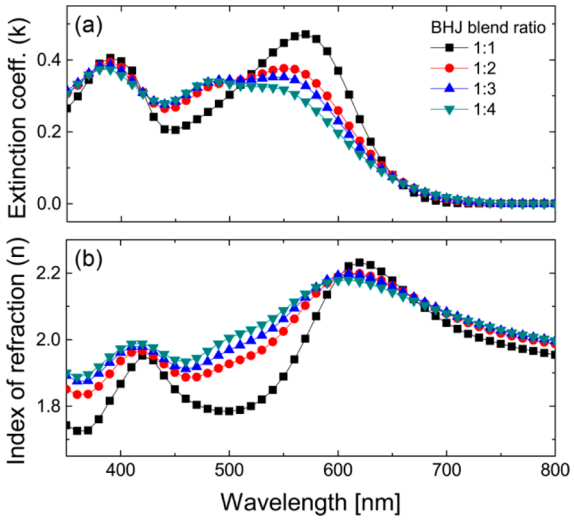

Figure 2. Spectral dependence of the optical constants measured by spectroscopic ellipsometry for blend ratios 1:1 to 1:4. Extinction coefficient k is shown in (a) and the refractive index n is presented in (b). These optical constants are necessary to simulate the optical field distribution in the whole device (as shown in Figure 3) and then to calculate the detailed light absorption in each layer of the solar cell stack.

containing 1:2, 1:3, and 1:4 blends all have very similar optical constants, while the 1:1 blend shows quite marked differences. From this data we surmise that the fullerene dominates the refractive index and extinction coefficient for ratios of 1:2 and greater. This would indicate that the EQE spectral changes as a function of blend ratio shown in Figure 1a are predominantly due to thickness effects. The results of transfer matrix calculations (optical field distribution and the number of absorbed photons at 532 nm) in two different junction thickness for the 1:4 blend are shown in Figure 3a [d = 80 nm] and b [d = 130 nm]. The optical field maximum at this wavelength (corresponding to one of the peaks in the EQE) moves through the cavity, and from the simulations one would predict that the optimal active layer thickness for the 1:4 blend is ~80 nm, which is indeed what we (and others) have observed empirically to be the case. In Figure 3c we plot the simulated photocurrent assuming 100% IQE (and weighted by the AM1.5G solar spectrum) as a function of cavity thickness. We also show for comparison the actual short circuit photocurrent measured in a number of cells with different active layer thicknesses in the same 1:4 blend system. Once again, we see the maximum photocurrent is predicted and observed with a junction of d = 80 nm. The simulated and measured photocurrents diverge in thicker active layers because increased recombination substantially reduces the IQE. This type of modeling is an invaluable tool in understanding where to begin the optimization process with a new material system and to assess the likely optical impacts of changing blend ratios and ancillary components such as electron and hole transporting layers.

Accurate Calculation of the Internal Quantum Efficiency (IQE). The EQE is strongly affected by the absorption characteristics of the junction as shown in Figure 1a,b. The IQE represents the solar cell response normalized by the number of photons actually absorbed by the active layer and hence contains information about the fundamental efficiency of the charge generation (exciton dissociation, charge transfer) and collection/extraction processes (recombination and transport, plus contact dynamics) versus the incident photon energy. For example, an incomplete charge transfer from the fullerene acceptor to the donor was reported by Burkhard et al.[37] in P3HT/PC60BM solar cells. The reported losses at high excitation energies where fullerene absorption is dominant were attributed to less efficient photoinduced hole transfer (the Channel II mechanism[36]). This is a clear example of how probing energy dependent charge generation by precisely acquiring the IQE leads to mechanistic insight. However, it is unfortunately all too common for IQE to be calculated from measured EQE without proper consideration of optical cavity and parasitic absorption effects. This was highlighted in a recent case where Grancini et al.[30] used an energy dependent IQE to support the observation of "hot excitons" in an organic solar cell composed of the acceptor–donor combination PCPDTBT/PC60BM. Armin et al.[31] and Scharber[32] both showed that if the IQE was calculated correctly by taking into account the relevant optical effects, the IQE was in fact invariant with respect to incident photon energy. In this particular case, Grancini et al. calculated the IQE by normalizing the EQE to the active layer absorption obtained by a simple film transmission measurement on glass[30] (Figure 4a). This simplistic analysis neglects the multilayer optical cavity phenomena described above and the parasitic absorptions in nonactive layers such as ITO, PEDOT/PSS, and the electrodes (PEDOT/PSS is poly(3,4-ethylenedioxythiophene)/poly(styrene sulfonate) and ITO is indium tin oxide). These parasitic absorptions can have strong wavelength dependent properties as demonstrated by the data presented in the Supporting Information (Figure S3).

Figure 4b shows a simple flowchart summarizing the various commonly used strategies for calculating the IQE. In the figure, the incorrect methods give an "IQE-like" spectrum with the correct procedure giving the "true-IQE" spectrum from the measured EQEs. In particular, it is critical to know the optical

dx.doi.org/10.1021/ph400044k | ACS Photonics 2014, 1, 173–181

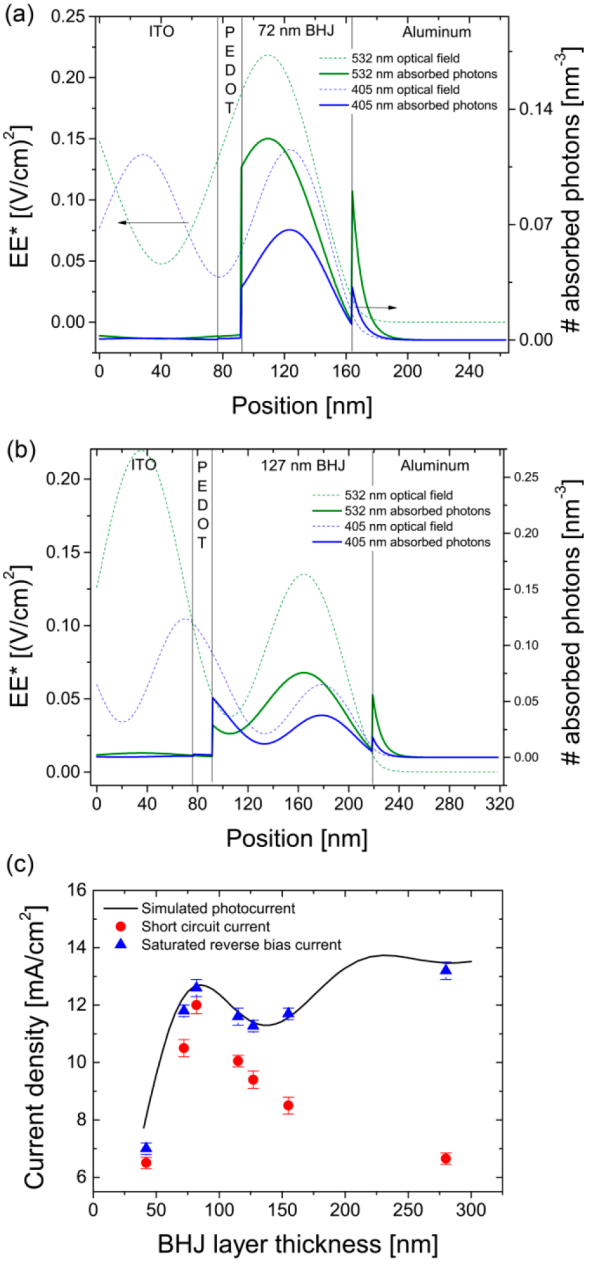

Figure 3. Simulated (transfer matrix method) optical field distributions and charge carrier photogeneration profiles in the each layer of the solar cell stack with active layer thicknesses of 72 nm (a) and 127 nm (b) evaluated at incident light wavelengths of 532 and 405 nm. Optical constants for the 1:4 blend ratio were used in these calculations. Due to optical interference, the light absorption profile in the active film does not follow the Beer–Lambert law and results in position dependent absorption peaks. (c) Simulated short circuit current (under AM1.5G as a function of active layer thickness with the assumption of IQE = 100% (solid line) and measured short circuit current (solid circles) for devices of different junction thicknesses). The differences between the simulated and measured short circuit currents are due to losses in charge transport (increased recombination) in thicker active layers where the IQE = 100% assumption breaks down. This is confirmed by the saturated reverse bias current (maximum achievable photocurrent), which follows closely the simulated photocurrent.

constants of all layers in the solar cell stack and to obtain an accurate near-normal incidence measurement of the device reflectance $[R(\lambda)]$. This reflectance encompasses the active layer absorption and also the effects of parasitic absorptions in the nonactive layers. Once again, transfer matrix simulations can be used to deconvolute the two and return an accurate value for the number of photons absorbed by the junction. From this, the "true-IQE" can be determined. The results of such an analysis for the PCPDTBT/PC60BM system previously mentioned are shown in Figure 5 where the individual panes follow the various steps outlined in Figure 4. Near-normal incidence reflectance spectra were obtained using a universal reflectance attachment (URA) on a Perkin-Elmer Lambda 950 spectrophotometer according to the procedure outlined in the Experimental Section and noting the care needed to accurately acquire baseline spectra. The outcomes (i.e., spectral dependencies of the IQEs) are very different depending on whether cavity interference and parasitic absorptions are correctly accounted for. The true-IQE for two active layer thicknesses (60 and 160 nm) are flat, whereas the IQE-like spectra show marked (and erroneous) energy dependencies. It is also worth noting that comparison of the full simulated reflectance of the solar cell stack and the measured near normal incidence reflectance serve as a means to check second order phenomena such as optical scattering from rough films and interfaces.[38] These are not captured by simple transfer matrix calculations but are manifest in experimental reflectance measurements as shown quite systematically by Burkhard et al.[39] The Burkhard protocol is very similar to the approach adopted here and considers all the key optical phenomena.

Returning now to the PCDTBT/PC70BM combination, the same process outlined in Figure 4b was applied to calculate the IQE from the EQE shown in Figure 1 as a function of both blend ratio and thickness. Figure 6a and b shows the true-IQE for the two single variable experiments, blend ratio and active layer thickness, respectively. In both cases, the IQE are spectrally flat (within the certainty of the measurement which we estimate to be ±6%, see Supporting Information) with maximum values exceeding 90% for the optimized cases (1:4 blend ratio and 70–100 nm junction thickness), as reported previously by Moon et al.[16] Thicker junctions are less efficient, as are blends <1:3. From such measurements we can conclude with some certainty that (i) the efficiencies of exciton dissociation and free carrier extraction in the optimized junctions are extremely high (>90%), one may say almost lossless; (ii) there appears to be no substantial energy dependence of the exciton dissociation process in PCDTBT/PC70BM blends (assuming carrier transport and extraction are likewise independent of the incident photon energy); and (iii) the Channel I (photoinduced electron transfer) and Channel II (photoinduced hole transfer) photocurrent generating pathways proceed with substantially the same efficiencies.[34,36] The decrease in IQE in thicker junctions greater than around 120 nm is consistent with low hole mobilities in PCDTBT, limiting the carrier extraction efficiency, as recently shown by Armin et al.[31] It is worthy of note that imbalanced charge transport derived from either very different electron and hole mobilities or a highly spatially asymmetric absorption profile can also have a pronounced effect on the efficiency of the charge carrier collection.[21] For example, in very thick junctions where the asymmetric absorption leads to a surface generation profile, one may expect a wavelength-dependent IQE. However, we did not observe such a dependence within the junction thickness range used in this work even though an optimized PCDTBT/PCBM blend has been shown to ~100× mobility imbalanced.[33]

Insight into the Relationship between Blend Ratio and Junction Thickness. The junction optical thickness as a function of incident photon energy, in addition to the perturbations caused by the parasitic layers define the cavity

dx.doi.org/10.1021/ph400044k | ACS Photonics 2014, 1, 173–181

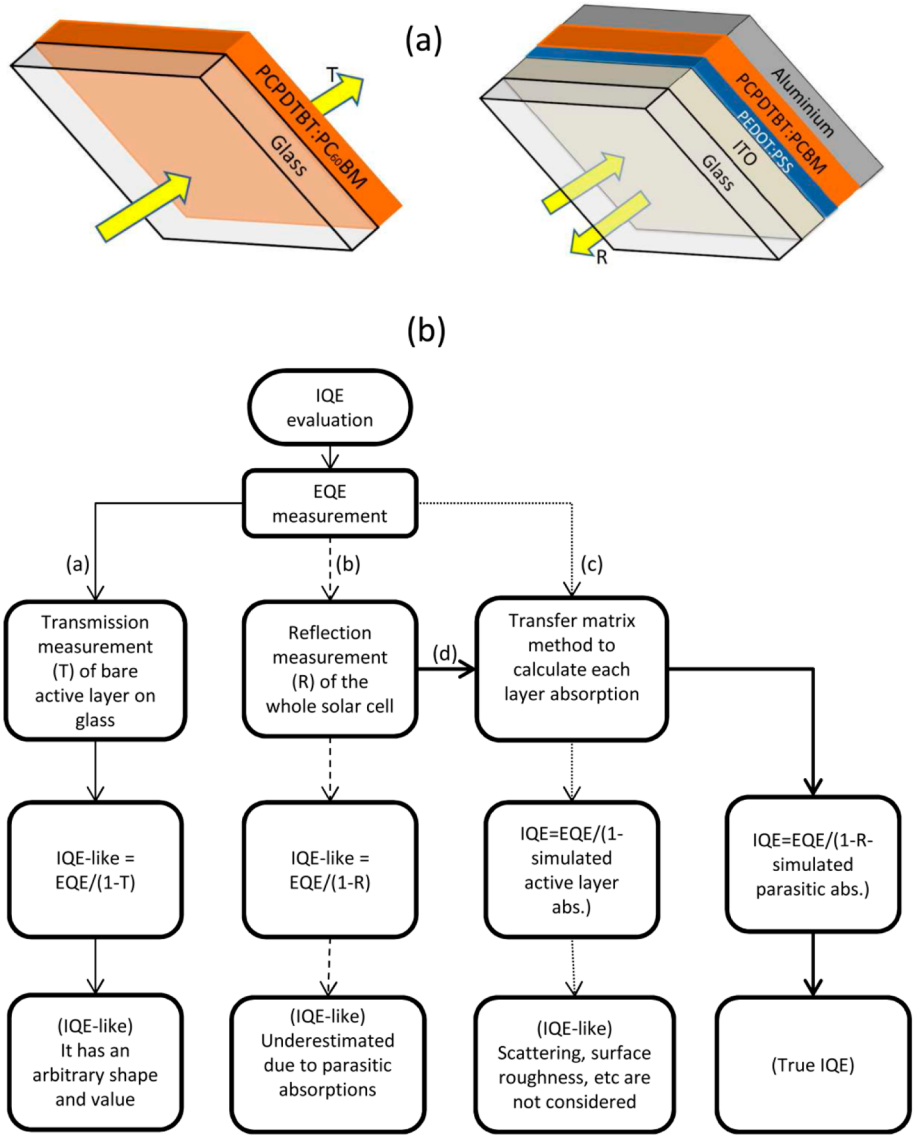

Figure 4. (a) Two different approaches for measuring the light absorption in the active layer of an organic solar cell. (Left) The active layer is deposited on a glass substrate and the absorption is determined from the simple UV−vis optical transmission. This approach neglects the cavity interference and parasitic absorptions present in the real solar cell stack. (Right) The measurement of the total reflectance of the device provides all of the relevant optical effects, and combined with an analysis of the parasitic absorptions, the amount of light absorbed by the active layer "in-device" can be accurately determined for the IQE calculations. (b) A simple flowchart showing the different approaches commonly used for IQE evaluation in thin film solar cells. Three of four different pathways in the flowchart result in an "IQE-like" spectrum which does not return the actual IQE of the solar cell. The true-IQE can only be obtained by fully accounting for all cavity interference and parasitic absorption effects.

optical field distribution. For blend ratios >1:1, the physical thickness of the active layer dominates $\eta_A(\lambda)$. However, as discussed previously, the blend ratio does have a significant impact upon the spin-casting solution viscosity (and therefore the resultant film thicknesses[40]) given that the system contains a high molecular weight polymer (PCDTBT) and a fullerene. Hence, to fundamentally assess the real effect of blend ratio on the efficiency of charge generation and extraction via the IQE, constant active layer thickness devices must be compared. In this regard, a film thickness calibration master curve is required for the spin coating process. Figure 7 shows the calibration master curve for PCDTBT/PC70BM, solution kinematic viscosities versus polymer concentration versus resultant film thickness obtained for a constant total solution concentration (see Experimental Section for measurement details). Reducing the polymer fraction substantially decreases the solution viscosity and hence the resultant active layer thickness. In contrast to PC70BM, PCDTBT polymer chains are significantly larger than the solvent molecules. This large difference in size results in frictional effects between the polymer and the solvent, increasing the solution viscosity with increasing polymer fraction.[41] In addition, at high PCDTBT fractions, physical entanglements between individual polymer chains further contribute to a significant increase in solution viscosities. The calibration curves of Figure 6 were used to create devices with almost identical active layer thickness (~80 nm) for blend ratios 1:1 to 1:4.

Figure 8a shows the EQE of these constant active layer thickness devices which confirms that the spectral responses are only weakly dependent upon blend ratio in contrast to the results presented in Figure 1a where the cavity thickness was not controlled. The respective IQEs are presented in Figure 8b and they confirm the beneficial effects of a high fullerene fraction in

dx.doi.org/10.1021/ph400044k | ACS Photonics 2014, 1, 173−181

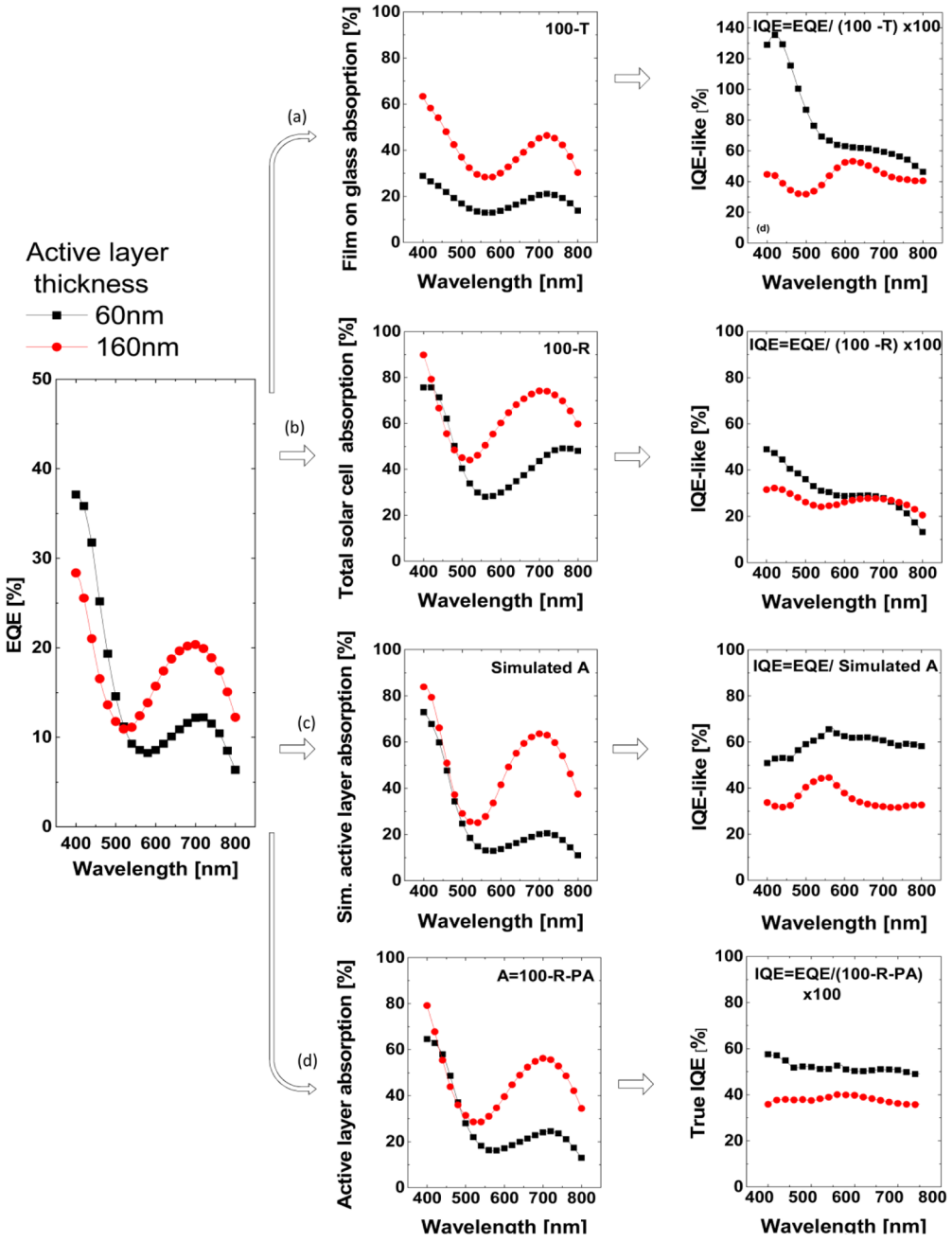

Figure 5. Demonstration of the four different pathways to calculating IQE, as outlined in the flowchart of Figure 4b. The example is shown for a PCPDTBT/PC60BM device (1:4 blend ratio) and for two junction thicknesses. Clearly there are dramatic differences between the simplest method based on absorption measurements of the active layer on glass and the most robust and accurate methodology, whereby the actual junction absorption via reflectance measurements and transfer matrix simulations are used. In the former case the IQE-like spectrum shows substantial energy dependence and in the latter the true-IQE is flat to within the error of the measurement (see Supporting Information), which is of order ±6%.

this system and the negative impact on charge generation and extraction yield of increased polymer concentration. In fully optimized PCDTBT/PC70BM organic solar cells there is no energy dependence of the internal quantum efficiency for charge carrier generation. This statement also holds true for PCPDTBT/PC60BM organic solar cells.

CONCLUSIONS

Cavity interference and parasitic absorptions in nonactive layers can dramatically impact the optical field distribution (and hence photogenerated carrier profile) in organic solar cells, which often have active layers thinner than where Beer–Lambert behavior predominates. We have demonstrated this principle for two model donor–acceptor bulk heterojunction systems namely PCDTBT/PC70BM and PCPDTBT/PC60BM. These effects must be understood and accounted for in "optimizing" a particular blend system, and modeling of the field distribution via transfer matrix simulations is a powerful tool in determining the best active layer thickness as a function of donor–acceptor ratio. Accurate simulations require detailed knowledge of the optical constants of all layers in the solar cell stack. We have also shown how such simulations in combination with near normal incidence reflection measurements can be used to accurately determine the "true-IQE" spectra from EQE measurements. Merely scaling the

dx.doi.org/10.1021/ph400044k | ACS Photonics 2014, 1, 173–181

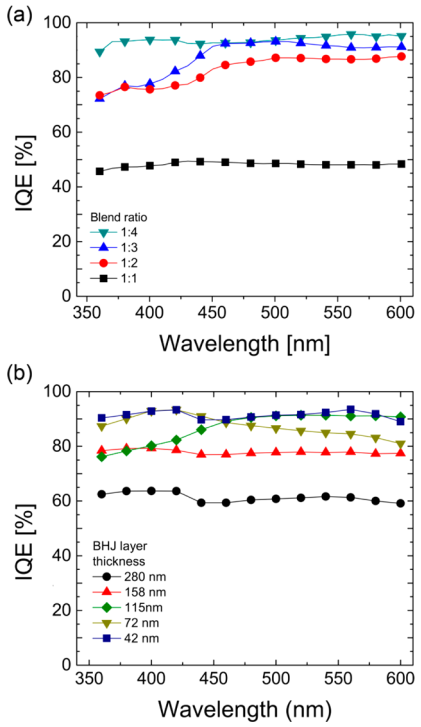

Figure 6. Internal quantum efficiency (IQE) spectra for PCDTBT/PC70BM organic solar cells as a function of blend ratio (a) and active layer thickness at a fixed blend ratio of 1:4 (b). These true-IQE spectra are spectrally flat (i.e., independent of the incident light energy within the measurement certainty of ±6%). The absolute values of the IQE indicate the relative efficiencies of the charge extraction and charge transfer state dissociation processes in each case. For example, for the 1:4 blend the extraction is relatively efficient up to a 127 nm junction thickness, but thicker films have more significant loss pathways.

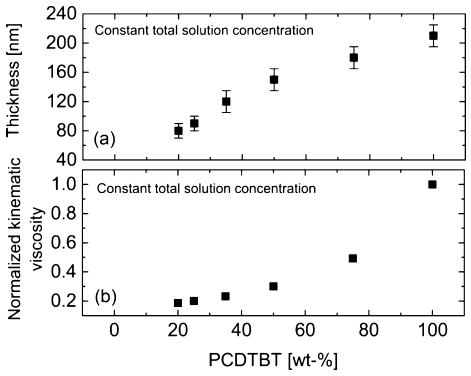

Figure 7. (a) Active layer thicknesses of PCDTBT/PC70BM organic solar cells (deposited at a constant spin speed) and (b) kinematic viscosities of the casting solution as a function of blend composition at constant material concentration (total concentration of both PCDTBT and PC70BM; cf. Figure 1b). With decreasing PCDTBT fraction in solution, kinematic viscosities, and hence, resulting thicknesses of the spin-coated active layers are reduced. This in turn directly affects the optical field distribution in the active layer of the solar cell.

measured EQE by the active layer absorption as determined from thin film on glass transmittance is inadequate and can lead to misleading "IQE-like" spectra with erroneous energy dependencies. These results highlight the importance of considering a thin film organic solar cell as a low finesse cavity; the coupling of optical and electronic effects defines the overall performance of these organic optoelectronic devices.

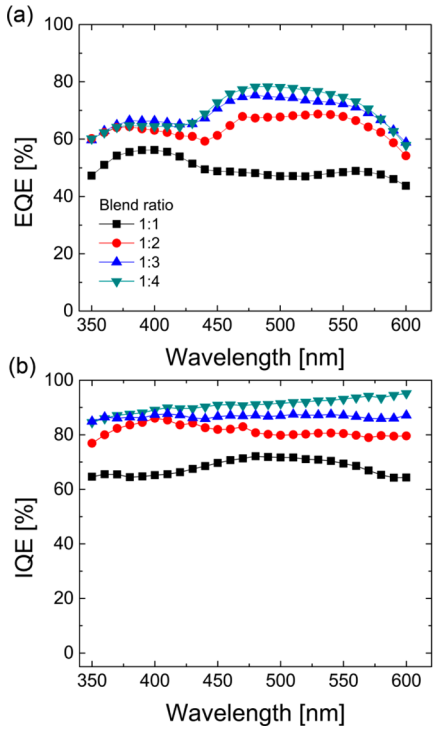

Figure 8. EQE (a) and IQE (b) spectra of PCDTBT/PC70BM organic solar cells with different active layer blend ratios (1:1 to 1:4) but similar thicknesses achieved by applying the calibration shown in Figure 7. The effect on the spectral shape of cavity interference effects arising from active layer thickness variations have been minimized in the EQE and the blend optical absorption is the dominant factor. As one would expect, the true-IQE are virtually flat and the reduced absolute IQE in the 1:1 blend is associated with a reduction in the extraction and charge transfer state dissociation efficiency.

EXPERIMENTAL SECTION

Solar Cell Device Fabrication. The 15 Ω/sq indium tin oxide coated glass substrates (Kintec) patterned by photolithography were precleaned by Alconox (detergent) solution and a soft cloth before being sonicated in sequence with Alconox, deionized water, acetone, and 2-propanol for 10 min, respectively. The cleaned substrates were coated with a 25 ± 5 nm layer of poly(3,4-ethylenedioxythiophene)/poly(styrene sulfonate) (PEDOT/PSS) purchased from Heraeus, by spin-casting at 5000 rpm for 60 s. The PEDOT/PSS layer was baked for 10 min at 170 °C. After that, a blend solution of polymer/fullerene was spin-coated with different concentrations and spin speeds depending on the polymer and blend ratio. The environmental conditions for fabrication were a nitrogen atmosphere (O_2 < 1 ppm, H_2O < 1 ppm) and a temperature of ∼20 °C. The thickness of the BHJ layer was measured by a Veeco Dektak 150 profilometer. Finally, 1 nm of samarium and 100 nm of aluminum were deposited to complete the device by thermal evaporation under a 10^{-6} mbar vacuum. The device area was 0.2 cm^2 with six devices per substrate.

PCDTBT/PC70BM Deposition. Poly[*N*-9″-heptadecanyl-2,7-carbazole-*alt*-5,5-(4′,7′-di-2-thienyl-2′,1′,3′-benzothiadiazole)] (PCDTBT) was synthesized and purified in-house following the Suzuki cross-coupling protocols previously described,[42] $\overline{M}_w$ = 33900 g/mol, PDI = 2.8, as determined from gel permeation chromatography (GPC) in 1,2,4-trichlorobenzene at 140 °C. Solutions of PCDTBT (30 mg/mL) and phenyl-C71-butyric acid methyl ester (PC70BM) (60 mg/mL)

dx.doi.org/10.1021/ph400044k | ACS Photonics 2014, 1, 173−181

were prepared separately in anhydrous 1,2-dichlorobenzene (DCB) by stirring at 90 °C and mixed after filtration with different volume ratios to obtain different blend ratios by weight. Blend ratios varied from 1:1 to 1:4 by weight. All the devices of Figure 1b were prepared from PCDTBT/PC70BM solutions with different blend ratio but total concentration of 35 mg/mL spun cast at 1000 rpm. Devices shown in Figure 8 were fabricated from solutions with different blend ratios and different total concentations. For 1:4, 1:3, 1:2, and 1:1 total concentrations (PCDTBT/PC70BM) were adjusted to 35, 30, 25, and 18 mg/mL, respectively, and spun-cast at 1000 rpm.

PCPDTBT/PC60BM Deposition. Poly[2,6-(4,4-bis-{2-ethylhexyl}-4*H*-cyclopenta[2,1-*b*;3,4-*b*′]-dithiophene)-*alt*-4,7-(2,1,3-benzothiadiazole)] (PCPDTBT) was synthesized and purified in house following the literature procedure described previously by Coffin et al.[43] ($\overline{M}_w = 1.4 \times 10^4$ and PDI = 1.3) and blended with phenyl-C61-butyric acid methyl ester (PC60BM) with a weight ratio of 1:4. The solutions of PCPDTBT and PC60BM were prepared separately in DCB at 90 °C and filtered before deposition. The total concentration was 40 mg/mL at a spin-casting speed of 600 rpm to obtain an active layer thickness of 160 nm and at 1500 rpm to obtain a 60 nm layer. Current−voltage curves and optical constants of PCPDTBT/PC60BM devices is presented in Supporting Information, Figures S4 and S5.

Solar Cell Efficiency Measurement. Light current−voltage curves were measured under simulated AM1.5G (~ 1000 W/m^2) illumination and the system was calibrated with a National Renewable Energy Laboratory (NREL)-certified standard 2 × 2 cm^2 silicon photodiode with a KG5 filter. A Keithley 2400 was used to record the data.

EQE Measurements and Spectroscopic Reflectometry. A PV Measurements Inc. QEX7 system was used for EQE measurements under an inert atmosphere. The EQE system was calibrated with a NIST calibrated silicone photodiode. Near-normal specular reflectance spectra of full solar cell stacks were obtained using a universal reflectance attachment (URA) on a Perkin-Elmer Lambda 950 spectrophotometer accurately baselined with a reference glass slab. Spectra were obtained over the relevant solar window 300−900 nm.

Spectroscopic Ellipsometry (SE). Silicon wafers with thickness of 1 mm were used as substrates for SE measurements of the optical constants. BHJ active layer films with different thicknesses ranging from 60 to 100 nm were spun-cast onto cleaned silicon wafers. The SE measurements were performed with a vacuum ultraviolet-variable angle spectroscopic ellipsometer (VUV-VASE; GEN II) J. A. Woollam with auto retarder. J. A.Woollam WVASE32 software was used for SE data analysis. A Cauchy model was initially used to obtain fitting parameters in the wavelength range of 900 to 1200 nm where the layers were almost transparent. Thereafter a point-to-point approach was chosen to obtain optical constants over the full scale (300−1200 nm).

Transfer Matrix Simulations To Obtain Parasitic Absorptions. A computational code based on the transfer matrix method[44] and developed by van de Lagemaat et al. from the National Renewable Energy Laboratory (NREL) was used to simulate the optical field distribution and absorptions in all stack layers. Additional details concerning the ellipsometry and optical model are presented in Zhang et al.[32]

Kinematic Viscosities (KV). KVs were determined using an Ostwald Micro Viscometer with a viscometer constant of 0.075. Solutions in the appropriate solvent were allowed to equilibrate at 20 °C for 15 min prior to measurement and viscosity values were averaged over 5 runs. More details concerning the Kinematic Viscosity measurements of PCDTBT/PC70BM solutions are discussed in ref 45 by the authors.

■ ASSOCIATED CONTENT

Supporting Information

The current−voltage curves for all the devices used in this work and the optical constants of the PCPDTBT/PC60BM devices that have been measured. The uncertainty of the IQE evaluation has also been estimated. This material is available free of charge via the Internet at http://pubs.acs.org.

■ AUTHOR INFORMATION

Corresponding Author

*E-mail: meredith@physics.uq.edu.au.

Notes

The authors declare no competing financial interest.

■ ACKNOWLEDGMENTS

A.A. is funded by a University of Queensland International scholarship (UQI). A.P. is the recipient of an Australian Research Council Discovery Early Career Researcher Award (Projects: ARC DECRA DE120102271, UQ ECR59-2011002311, and UQ NSRSF-2011002734). P.M. and P.L.B. are Vice Chancellor's Senior Research Fellows. P.W. would like to thank the Swiss National Science Foundation (SNSF) for an Advanced Researcher Fellowship (PA00P2_145395). We acknowledge funding from the University of Queensland (Strategic Initiative, Centre for Organic Photonics and Electronics), the Queensland Government (National and International Research Alliances Program), and the ARC Centre of Excellence for Antimatter−Matter Studies. This work was performed in part at the Queensland node of the Australian National Fabrication Facility (ANFF), a company established under the National Collaborative Research Infrastructure Strategy to provide nano- and microfabrication facilities for Australia's researchers. The authors kindly thank SJPC, Canada, for providing sample PCDTBT material and for performing the high-temperature GPC analyses. This Program has also been supported by the Australian Government through the Australian Renewable Energy Agency (ARENA). Responsibility for the views, information, or advice expressed herein is not accepted by the Australian Government.

■ REFERENCES

(1) Li, W.; Hendriks, K. H.; Roelofs, W. S.; Kim, Y.; Wienk, M. M.; Janssen, R. A. Polymer solar cells: Efficient small bandgap polymer solar cells with high fill factors for 300 nm thick films. *Adv. Mater.* **2013**, *25*, 3256−3256.

(2) Seo, J. H.; Gutacker, A.; Sun, Y.; Wu, H.; Huang, F.; Cao, Y.; Scherf, U.; Heeger, A. J.; Bazan, G. C. Improved high-efficiency organic solar cells via incorporation of a conjugated polyelectrolyte interlayer. *J. Am. Chem. Soc.* **2011**, *133*, 8416−8419.

(3) He, Z.; Zhong, C.; Su, S.; Xu, M.; Wu, H.; Cao, Y. Enhanced power-conversion efficiency in polymer solar cells using an inverted device structure. *Nat. Photon.* **2012**, *6*, 593−597.

(4) Li, J.; Zhao, Y.; Tan, H. S.; Guo, Y.; Di, C.-A.; Yu, G.; Liu, Y.; et al. A stable solution-processed polymer semiconductor with record high-mobility for printed transistors. *Sci. Rep.* **2012**, *2*, 1−9.

(5) Jung, J.; Liu, W. F.; Russell, T. P.; Jo, W. H. A high mobility conjugated polymer based on dithienothiophene and diketopyrrolopyrrole for organic photovoltaics. *Energy Environ. Sci.* **2012**, *5*, 56857−6861.

(6) Koppe, M.; Egelhaaf, H. J.; Dennler, G.; Scharber, M. C.; Brabec, C. J.; Schilinsky, P.; Hoth, C. N. Near IR sensitization of organic bulk heterojunction solar cells: towards optimization of the spectral response of organic solar cells. *Adv. Funct. Mater.* **2012**, *20*, 338−346.
(7) Kim, J. B.; Kim, P.; Pegard, N. C.; Oh, S. J.; Kagan, C. R.; Fleischer, J. W.; Stone, H. A.; Loo, Y.-L. Wrinkles and deep folds as photonic structures in photovoltaics. *Nat. Photon.* **2012**, *6*, 327−332.
(8) Kim, S. J.; Margulis, G. Y.; Rim, S. B.; Brongersma, M. L.; McGehee, M. D.; Peumans, P. Geometric light trapping with a V-trap for efficient organic solar cells. *Opt. Express* **2013**, *21*, A305−A312.
(9) Pandey, A. K.; Aljada, M.; Velusamy, M.; Burn, P. L.; Meredith, P. Nanostructured, active organic−metal junctions for highly efficient charge generation and extraction in polymer-fullerene solar cells. *Adv. Mater.* **2012**, *24*, 1055−1061.
(10) Kyaw, A. K. K.; Wang, D. H.; Tseng, H.-R.; Zhang, J.; Bazan, G. C.; Heeger, A. J. Electron and hole mobility in solution-processed small molecule-fullerene blend: dependence on the fullerene content. *Appl. Phys. Lett.* **2013**, *102*, 163308.
(11) Graham, K. R.; Wieruszewski, P. M.; Stalder, R.; Hartel, M. J.; Mei, J.; So, F.; Reynolds, J. R. Improved performance of molecular bulk-heterojunction photovoltaic cells through predictable selection of solvent additives. *Adv. Funct. Mater.* **2012**, *22*, 4801−4813.
(12) Shockley, W.; Queisser, H. J. Detailed balance limit of *p*−*n* junction solar cells. *J. Appl. Phys.* **1961**, *32*, 510−519.
(13) Forrest, S. R. The limits to organic photovoltaic cell efficiency. *MRS Bull.* **2005**, *30*, 28−32.
(14) Juška, G.; Arlauskas, K.; Viliūnas, M.; Genevičius, K. Charge transport in π-conjugated polymers from extraction current transients. *Phys. Rev. B* **2000**, *62*, R16235−R16238.
(15) Park, S. H.; Roy, A.; Beaupre, S.; Cho, S.; Coates, N.; Moon, J. S.; Moses, D.; Leclerc, M.; Lee, K.; Heeger, A. J. Bulk heterojunction solar cells with internal quantum efficiency approaching 100%. *Nat. Photonics* **2009**, *3*, 297−302.
(16) Moon, J. S.; Jo, J.; Heeger, A. J. Nanomorphology of PCDTBT:PC70BM bulk heterojunction solar cells. *Adv. Energy Mater.* **2012**, *2*, 304−308.
(17) Pivrikas, A.; Neugebauer, H.; Sariciftci, N. S. Charge carrier lifetime and recombination in bulk heterojunction solar cells. *IEEE J. Sel. Top. Quant. Electron.* **2010**, *16*, 1746−1758.
(18) Sievers, D. W.; Shrotriya, V.; Yang, Y. Modeling optical effects and thickness dependent current in polymer bulk-heterojunction solar cells. *J. Appl. Phys.* **2006**, *100*, 114509−114509.
(19) Ameri, T.; Dennler, G.; Waldauf, C.; Denk, P.; Forberich, K.; Scharber, M. C.; Brabec, C. J.; Hingerl, K. Realization, characterization, and optical modelling of inverted bulk-heterojunction organic solar cells. *J. Appl. Phys.* **2008**, *103*, 084506−084506.
(20) Nickel, F.; Sprau, C.; Klein, M. F.; Kapetana, P.; Christ, N.; Liu, X.; Klinkhammer, S.; Lemmer, U.; Colsmann, A.. Spatial mapping of photocurrents in organic solar cells comprising wedge-shaped absorber layers for an efficient material screening. *Sol. Energy Mater. Sol. Cells* **2012**, *104*, 18−22.
(21) Mescher, J.; Christ, N.; Kettlitz, S.; Colsmann, A.; Lemmer, U. Influence of the spatial photocarrier generation profile on the performance of organic solar cells. *Appl. Phys. Lett.* **2012**, *101*, 073301−073301.
(22) Mihailetchi, V. D.; Koster, L. J. A.; Blom, P. W. M.; Melzer, C.; de Boer, B.; van Duren, J.K. J.; Janssen, R. A. J. Compositional dependence of the performance of poly(*p*-phenylene vinylene): methanofullerene bulk-heterojunction solar cells. *Adv. Funct. Mater.* **2005**, *15*, 795−801.
(23) Yao, Y.; Hou, J.; Xu, Z.; Li, G.; Yang, Y. Effects of solvent mixtures on the nanoscale phase separation in polymer solar cells. *Adv. Funct. Mater.* **2008**, *18*, 1783−1789.
(24) Ma, W.; Kim, J. Y.; Lee, K.; Heeger, A. J. Effect of the molecular weight of poly(3-hexylthiophene) on the morphology and performance of polymer bulk heterojunction solar cells. *Macromol. Rapid Commun.* **2007**, *28*, 1776−1780.
(25) Schilinsky, P.; Asawapirom, U.; Scherf, U.; Biele, M.; Brabec, C. J. Influence of the molecular weight of poly(3-hexylthiophene) on the performance of bulk heterojunction solar cells. *Chem. Mater.* **2005**, *17*, 2175−2180.
(26) Seo, J. H.; Nam, S. Y.; Lee, K.-S.; Kim, T.-D.; Cho, S. The effect of processing additive on aggregated fullerene derivatives in bulk-heterojunction polymer solar cells. *Org. Electron.* **2012**, *13*, 570−578.
(27) Taima, T.; Sakai, J.; Yamanari, T.; Saito, K. Doping effects for organic photovoltaic cells based on small-molecular-weight semiconductors. *Sol. Energy Mater. Sol. Cells* **2009**, *93*, 742−745.
(28) Dennler, G.; Forberich, K.; Scharber, M. C.; Brabec, C. J.; Tomis, I.; Hingerl, K.; Fromherz, T. Angle dependence of external and internal quantum efficiencies in bulk-heterojunction organic solar cells. *J. Appl. Phys.* **2007**, *102*, 054516−054516.
(29) Gowrishankar, V.; Scully, S. R.; McGehee, M. D.; Wang, Q.; Branz, H. M. Exciton splitting and carrier transport across the amorphous-silicon/polymer solar cell interface. *Appl. Phys. Lett.* **2006**, *89*, 52102−252102.
(30) Grancini, G.; Maiuri, M.; Fazzi, D.; Petrozza, A.; Egelhaaf, H. J.; Brida, D.; Cerullo, G.; Lanzani, G. Hot exciton dissociation in polymer solar cells. *Nat. Mater.* **2013**, *12*, 29−33.
(31) Armin, A.; Zhang, Y.; Burn, P. L.; Meredith, P.; Pivrikas, A. Measuring internal quantum efficiency to demonstrate hot exciton dissociation. *Nat. Mater.* **2013**, *12*, 593−593.
(32) Scharber, M. C. Measuring internal quantum efficiency to demonstrate hot exciton dissociation. *Nat. Mater.* **2013**, *12*, 594−594.
(33) Armin, A.; Juska, G.; Ullah, M.; Velusamy, M.; Burn, P. L.; Meredith, P.; Pivrikas, A. Balanced carrier mobilities: not a necessary condition for high efficiency thin organic solar cells as determined by MIS-CELIV. *Adv. Energy Mater.* **2013**, DOI: 10.1002/aenm.201300954.
(34) Zhang, Y.; Pandey, A. K.; Tao, C.; Fang, Y.; Jin, H.; Burn, P. L.; Meredith, P. Spectral response tuning using an optical spacer in broad-band organic solar cells. *Appl. Phys. Lett.* **2013**, *102*, 013302.
(35) Kim, J. Y.; Kim, S. H.; Lee, H.-H.; Lee, K.; Ma, W.; Gong, X.; Heeger, A. J. New architecture for high-efficiency polymer photovoltaic cells using solution-based titanium oxide as an optical spacer. *Adv. Mater.* **2006**, *18*, 572−576.
(36) Fang, Y.; Pandey, A. K.; Nardes, A. M.; Kopidakis, N.; Burn, P. L.; Meredith, P. A narrow optical gap small molecule acceptor for organic solar cells. *Adv. Energy Mater.* **2013**, *3*, 54−59.
(37) Burkhard, G. F.; Hoke, E. T.; Scully, S. R.; McGehee, M. D. Incomplete exciton harvesting from fullerenes in bulk heterojunction solar cells. *Nano Lett.* **2009**, *9*, 4037−4041.
(38) Wang, D. H.; Kim, D. Y.; Choi, K. W.; Seo, J. H.; Im, S. H.; Park, J. H.; Park, O. O.; Heeger, A. J. Enhancement of donor−acceptor polymer bulk heterojunction solar cell power conversion efficiencies by addition of Au nanoparticles. *Angew. Chem.* **2011**, *123*, 5633−5637.
(39) Burkhard, G. F.; Hoke, E. T.; McGehee, M. D. Accounting for interference, scattering, and electrode absorption to make accurate internal quantum efficiency measurements in organic and other thin solar cells. *Adv. Mater.* **2010**, *22*, 3293−3297.
(40) Van Bavel, S. S.; Bärenklau, M.; Hoppe, H.; Loos, J. P3HT/PCBM bulk heterojunction solar cells: impact of blend composition and 3D morphology on device performance. *Adv. Funct. Mater.* **2010**, *20*, 1458−1463.
(41) de Gennes, P. D. Stochastic-molecular theory of spin−relaxation for liquid crystals. *J. Chem. Phys.* **1977**, *66*, 5825−5826.
(42) Blouin, N.; Michaud, A.; Gendron, D.; Wakim, S.; Blair, E.; Neagu-Plesu, R.; Belletête, M.; Durocher, G.; Tao, Y.; Leclerc, M. Toward a rational design of poly(2,7-carbazole) derivatives for solar cells. *J. Am. Chem. Soc.* **2008**, *130*, 732.
(43) Coffin, R. C.; Peet, J.; Rogers, J.; Bazan, G. C. Streamlined microwave-assisted preparation of narrow-bandgap conjugated polymers for high-performance bulk heterojunction solar cells. *Nat. Chem.* **2009**, *1*, 657−661.
(44) Peumans, P.; Yakimov, A.; Forrest, S. R. Small molecular weight organic thin-film photodetectors and solar cells. *J. Appl. Phys.* **2003**, *93*, 3693.
(45) Wolfer, P.; Armin, A.; Pivrikas, A.; Velusamy, M.; Burn, P. L.; Meredith, P. Solution structure: defining polymer film morphology and optoelectronic device performance. *J. Mater. Chem. C* **2013**, *2*, 71.